Trade-off in production between adjacent seamount chains near the East Pacific Rise

Yang Shen*†, Daniel S. Scheirer‡§, Donald W. Forsyth* & Ken C. Macdonald‡

* Department of Geological Sciences, Brown University, Providence, Rhode Island 02912, USA
‡ Department of Geological Sciences, University of California, Santa Barbara, California 93106, USA

BATHYMETRIC data and side-scan sonar images collected near the southern East Pacific Rise between 15° and 19° S[1,2] have revealed many seamounts on the west flank of the rise, most of which are organized into chains running perpendicular to the rise axis. The number of seamounts of >5 km diameter is at least twice that expected for average East Pacific sea floor[3]. The formation of numerous, small (<2,500 m in relief) seamounts in ocean basins has been a subject of study for many years[3–10], yet we have little understanding of how magma is generated and supplied to build the seamounts. Here we report that the production of seamounts in closely spaced (20–25 km), adjacent seamount chains is negatively correlated, suggesting that the chains share common sources. The existence of closely spaced, long-lived (>5 Myr), linear seamount chains and the tendency for fresh lava flows to be found primarily at the near-ridge ends of the chains suggest that there are plume-like sources in the upper mantle, which are relatively stationary, active for extended periods and affected by adjacent sources.

Most seamounts on the west flank of the southern East Pacific Rise originate within 30 km of the ridge axis[1]. In the initial, small study area that we surveyed during December 1990 and January 1991, fresh lava flows are only seen at the axial ends of three major seamount chains (Fig. 1*a*), indicating that the seamounts are formed near the ridge axis, then passively carried away from the East Pacific Rise by the motion of the Pacific plate at a rate of 70 km Myr^{-1} (ref. 11). Because the primary seamount building activity occurs from 10 to 50 km off-axis, seamount volume as a function of distance from the ridge may be interpreted to a first approximation as variations in volcanic production or extrusion rate as a function of time. In the initial study area, the largest seamounts are at the western end of the Chapple seamount chain, the centre of the Anakena chain, and the eastern end of the Toroko chain (Fig. 1*a*). Based on this limited data set, we hypothesized that an increase in the volume of one chain is at the cost of the volume of adjacent chains at similar distances from the axis[1]. We suggested that, if this hypothesis holds up with more data, then these seamount chains may share a common source.

Additional bathymetric and side-scan sonar data to test this hypothesis were obtained during November and December of 1992 in an area about 10 times as large as the original survey[2]. We restrict our analysis to the part of the survey area that has nearly continuous bathymetric coverage along the chains, extending from the southern EPR ~340 km off-axis (Fig. 1*b*). Side-scan sonar images, which have a 20-km wide swath, indicate that no major seamount edifices are missed in gaps of the bathymetric coverage. We divide the seamount field into six equally spaced corridors to minimize subjective grouping of seamount chains. The geometry of the corridors is based primarily on the nearly continuous Cloud chain. In this simple way of dividing the seamount field, no major seamount chains cross the boundaries of the corridors. In general, seamount volcanism within corridors is more continuous than appears in Fig. 1, with small seamounts or lava flows between major edifices that can be recognized on detailed bathymetry or side-scan sonar maps.

Qualitatively, the additional data appear to support our hypothesis (Fig. 1*b*): at about 114.5° W, where the Anakena corridor is voluminous, the Toroko and the Chapple corridors have only minor volcanic construction; at about 115° W, where volume in the Toroko corridor is at its peak, there are only minor seamounts in the Chapple and Anakena corridors; further west, where volume in the Chapple corridor is maximum, the Toroko corridor is at a minimum. One exception is at about 116° W where there are voluminous chains in both the Ruru and Chapple corridors. Quantitative analyses (see below), may be used to test whether the apparent negative correlation between volcanism in adjacent chains is statistically significant.

The volumes of seamount edifices within individual corridors fluctuate substantially with distance from the axis (Fig. 2*a*). Their sum shows a rapid increase in volume in the first 60 km from the ridge axis, then appears to behave as a random deviation from a mean that may increase slightly with crustal age. Side-scan sonar data show that there is minor volcanic activity off-axis (>60 km) in this area that continues to increase the volume of existing edifices, perhaps linking adjacent seamounts in a chain together into ridges[2]. The primary seamount building activity in these chains, however, occurs within 60 km of the axis. To determine whether the observed correlation of volumes of adjacent seamount corridors is significant, we constructed simulated seamount corridors that have the same statistical volume variations as the observed corridors, but which vary independently between each other in volcanic activity. By comparing the observed correlations to correlations of the simulated seamount corridors, we can test the probability that the observed correlations could have arisen by chance. We use simulated corridors for comparison, because the variations in volume for individual corridors are not normally distributed and standard, simple statistical tests based on the assumption of normality cannot be applied directly.

Figure 2*b* shows an example of a simulated seamount corridor. The simulated corridors share the following statistical characteristics with the real corridors: the ratio of number of positive points to number of zero points, standard deviation, skewness and kurtosis. The only difference between the observed and the simulated corridors is that extrusion rate of each simulated corridor is independent of the others, whereas the extrusion rate of real seamounts may be coherent between adjacent corridors.

We cross-correlated the simulated seamount corridors with each other to obtain a cumulative distribution function (c.d.f.) of the cross-correlation coefficients (Fig. 2*c*). We then cross-correlated immediately adjacent real seamount corridors and projected the correlation coefficients on the c.d.f. curve (solid dots, Fig. 2*c*). Four out of five correlation coefficients are negative and fall in the lower half of the distribution; three are in the lowest 3%. The lone instance in the upper half of the distribution is the correlation between the Chapple and the Ruru corridors, the exception pointed out above. The mean of the five coefficients is −0.10, compared to the mean of 0.08 from the randomly varying simulations. A Student's *t*-test indicates that this mean for adjacent corridors is different from the mean for independent corridors at the 99.6% confidence level, and this estimate of confidence level is confirmed by constructing another c.d.f. for the means of groups of five independent correlations.

The cross-correlation of one corridor with another one at least two corridors apart yields three points in the lower half of the distribution and three points in the upper half (open circles, Fig. 2*c*). Their mean is not significantly different from the mean of the correlations between simulated corridors, suggesting that negative correlation may only exist between adjacent seamount corridors.

† Present address: Department of Geology and Geophysics, Woods Hole Oceanographic Institution, Woods Hole, Massachusetts 02543, USA.
§ Present address: Department of Geological Sciences, Brown University, Providence, Rhode Island 02912, USA.

The statistical tests indicate that negative correlation between volumes of adjacent seamount corridors is significant at a high confidence level. The most probable explanation for such a negative correlation is that adjacent seamount chains share a common source that is roughly constant in volume per unit time[1] (Fig. 2*a*). Several mechanisms may be responsible for seamount volcanism. They include small-scale, ridge-perpendicular convection[12,13], north–south extension of the lithosphere[14,15], upwelling associated with plate spreading[8], preferential melting of heterogeneities embedded within the upwelling mantle beneath the ridge[6,16], magmatic solitary waves generated in the primary melt production region[17], and mini-plumes with sources in the deep mantle[1,7,9]. Stresses within the lithosphere associated with seamount formation may also affect the likelihood that magma can penetrate through adjacent lithosphere[14,18,19]. The fact that such closely spaced, long-lived, linear seamount chains have not been observed in other ridge-flank surveys[20] suggests that their occurrence may be related to a mechanism that is not common to all ridges. Our conclusions apply only to the dominant, near-axis activity in the Rano Rahi field. Other, farther off-axis, volcanism could be caused by other mechanisms[3,15,21] and, if superimposed on the edifices created near-axis, would degrade the observed negative correlations.

The existence of linear chains, the tendency for fresh lava flows to be found primarily at the near-ridge ends, and the correlation in volume between adjacent chains suggest that there are sources within the mantle that are nearly stationary relative to the ridge, active for an extended period (>5 Myr), and affected by adjacent sources. It is difficult to see how passively embedded heterogeneities could cause coordinated waxing and waning of adjacent chains[1]. However, trade-offs in production might arise from plume-forming thermal or chemical instabilities at a boundary layer in the mantle (Fig. 3). We suggest that mini-plumes and trailing conduits developed from the instability. Disturbances generated within the boundary layer repeatedly travel up the conduits, producing fluctuations in discharge within each plume[22]. As the conduit wave reaches the depth where pressure-release melting begins, a large volume of magma is produced and extracted to form seamounts. Between conduit waves, the magma supply is limited and either no edifices are formed or only small cones are built. Increase in flux to one conduit may drain material from the surrounding source area, causing a decrease in flux to adjacent conduits. With the large number and relatively close spacing of seamount chains, it is unlikely that the instability is at the core–mantle boundary. The instability could be in the upper-mantle transition zone, in the astheno-

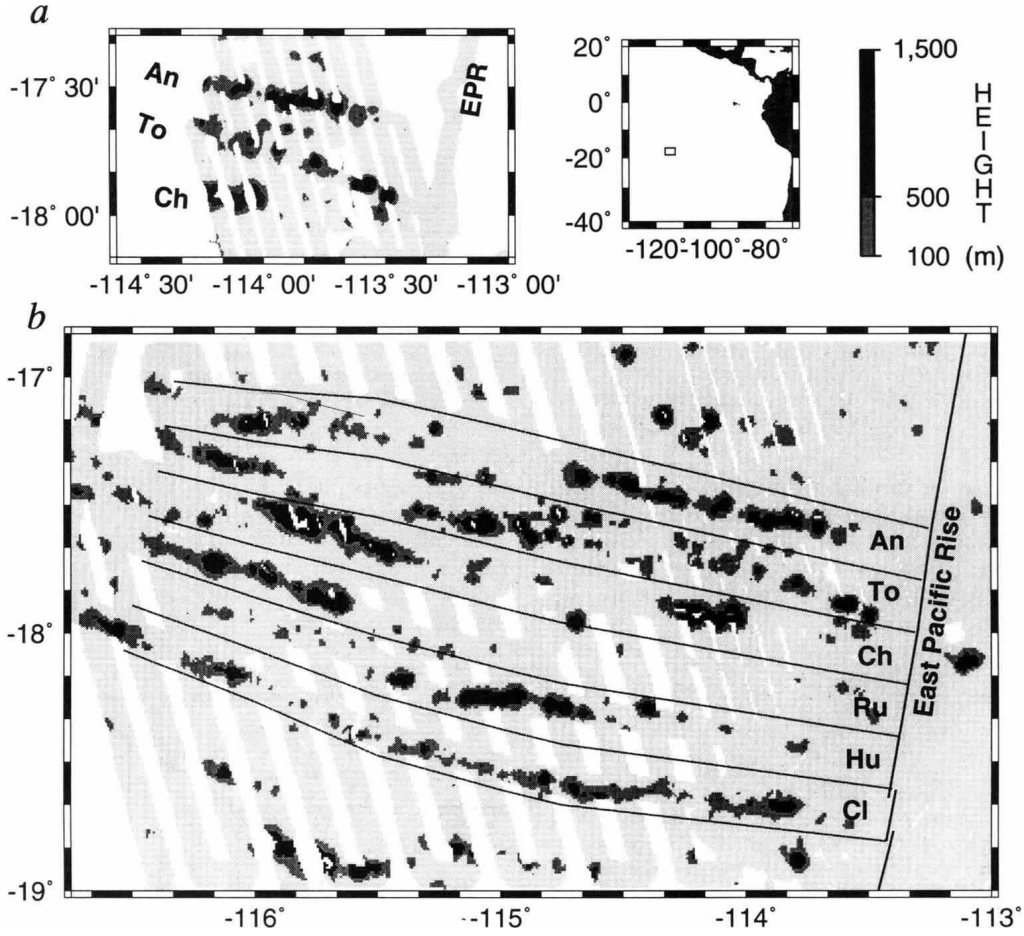

FIG. 1 Distribution of seamounts on the west flank of the East Pacific Rise. Shaded regions indicate continuous bathymetric coverage from SeaBeam2000 multibeam sonar data. Side-scan sonar coverage, from HMR1, is nearly 100%. Darker shades represent the relief of seamounts (m above sea floor, see scale bar) isolated from bathymetric data with an anisotropic median filter[1], which are at least 100 m shallower than the surrounding sea floor. Small-scale map shows location of survey area relative to South America and ridge axes. *a*, Distribution of the three major seamount chains mapped during December 1990 and January 1991. *b*, The Rano Rahi seamount field mapped primarily during November and December 1992, but including older data as well. The part of the seamount field which has continuous coverage along the seamount chains is divided into six equally spaced corridors, delineated by solid lines. Although some of the seamount chains bifurcate and most of the corridors contain more than one distinct chain, no major groups of seamounts cross the boundaries of the corridors. The Anakena, Toroko, Chapple, Ruru, Hurihuri and Cloud seamount corridors are labelled with two-character symbols standing for the name of the most prominent chain within each corridor.

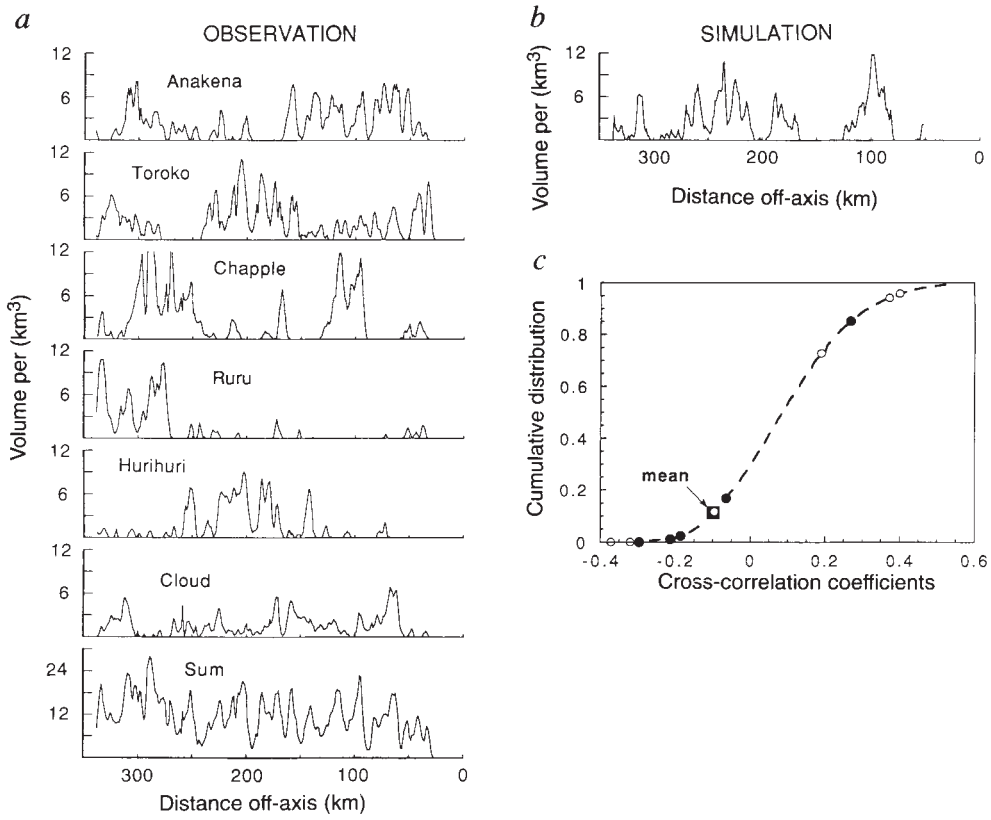

FIG. 2 Comparison of real and simulated seamount chains. *a*, Variation in volume of individual corridors (see Fig. 1) and the sum of the six seamount corridors. Volume per unit distance along the corridors is measured in 1-km bins. *b*, Variation in volume of one of 120 simulated seamount corridors. These were simulated with a fourth-order autoregressive function, $V(t)=a_1V(t-1)+a_2V(t-2)+a_3V(t-3)+a_4V(t-4)+Z(t)$, where $Z(t)$ is a gaussian, random, input variable, V is the volume at time (or, equivalently, distance) t, and the coefficients, a_i, are determined by least-squares fit to the observed, non-zero values of seamount volume at distances >50 km from the ridge axis. Based on partial correlation functions[25], higher-order terms are unnecessary. The output from the autoregressive function is then corrected to the observed cumulative distribution function of volume versus distance, including a non-negative constraint. *c*, Cumulative distribution function (dashed curve) of 7,140 cross-correlation coefficients of simulated seamount corridors. Note that the cross-correlation coefficients are not normally distributed because the variations in volume for individual corridors are not normally distributed. The cross-correlation coefficients of the real, immediately adjacent corridors are projected on the curve as solid dots. Their mean is shown as the solid square. The coefficients of one corridor with another one at least two corridors apart are projected on the curve as open circles.

sphere or at the base of the melting region, although it may be more difficult for sources at shallowest levels to be relatively stationary for an extended period of time in a vigorously upwelling environment. Based on Rayleigh–Taylor instability theory[23,24] and the spacing between seamount chains (20–25 km), we estimate that the thickness of the unstable layer is of the order of a few kilometres and the viscosity of the instability layer ($<10^{17}$ Pa s) is much smaller than that of the upper mantle. The unstable layer could also be a potential source for seamounts on the Nazca plate, but with current bathymetric

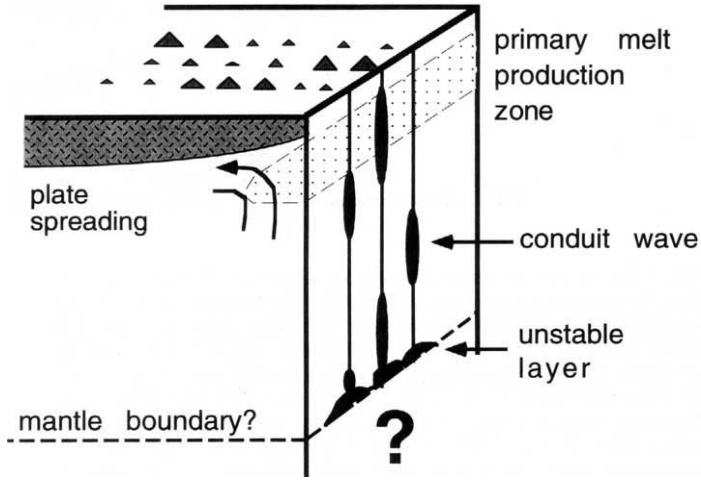

FIG. 3 Schematic diagram showing preferred model for the formation of the negatively correlated seamount chains. The cross-section parallel to the ridge axis is slightly off-axis. Triangles represent seamounts. Arrow and curves represent upwelling flow associated with plate spreading. The 'primary melt production zone' is the region in which mantle melts to form depleted mid-ocean-ridge basalts. Disturbances generated within a thermal or chemical instability layer travel as waves up the conduit, producing fluctuations in discharges within each plume. Increase in flux to one conduit may drain material from the surrounding region of the unstable layer, causing a decrease in flux to adjacent conduits. Depth of the instability is unkown, although it is not likely to be at the core–mantle boundary.

coverage, it is not clear whether similar chains exist to the east of the East Pacific Rise axis. □

Received 28 July; accepted 22 November 1994.

1. Shen, Y., Forsyth, D. W., Scheirer, D. S. & Macdonald, K. C. *J. geophys. Res.* **98,** 17875–17889 (1993).
2. Scheirer, D. S., Macdonald, K. C., Forsyth, D. W. & Shen, Y. *Mar. Geophys. Res.* (submitted).
3. Smith, D. K. & Jordan, T. H. *J. geophys. Res.* **93,** 2899–2918 (1988).
4. Simkin, T. *Mem. geol. Soc. Am.* **132,** 183–193 (1972).
5. Fornari, D. J., Ryan, W. B. F. & Fox, P. J. *J. geophys. Res.* **89,** 11609–11083 (1984).
6. Davis, E. E. & Karsten, J. L. *Earth planet. Sci. Lett.* **79,** 385–396 (1986).
7. Barone, A. M. & Ryan, W. B. F. *J. geophys. Res.* **95,** 10801–10827 (1990).
8. Batiza, R., Niu, Y. & Zayac, W. C. *Geology* **18,** 1122–1125 (1990).
9. Desonie, D. L. & Duncan, R. A. *J. geophys. Res.* **95,** 12697–12711 (1990).
10. Bemis, K. G. & Smith, D. K. *Earth planet. Sci. Lett.* **118,** 251–262 (1993).
11. Cormier, M.-H. & Macdonald, K. C. *J. geophys. Res.* **99,** 543–564 (1994).
12. Haxby, W. F. & Weissel, J. K. *J. geophys. Res.* **91,** 3507–3520 (1986).
13. Buck, W. R. & Parmentier, E. M. *J. geophys. Res.* **91,** 1961–1974 (1986).
14. Winterer, E. L. & Sandwell, D. T. *Nature* **329,** 534–537 (1987).
15. Sandwell, D. T. *et al. J. geophys. Res.* (submitted).
16. Wilson, D. *Earth planet. Sci. Lett.* **113,** 41–55 (1992).
17. Spiegelman, M. & Winggins, C. (abstr.) *EOS* **74,** 684 (1993).
18. ten Brink, U. *Geology* **19,** 397–400 (1991).
19. Macdonald, K. C. *Nature* **331,** 395 (1988).
20. Scheirer, D. S. & Macdonald, K. C. *J. geophys. Res.* (in the press).
21. McNutt, M. K. & Fisher, K. M. *Seamounts, Islands, and Atolls* 25–34 (Geophys. Monogr. No. 43, Am. Geophys. Union, Washington DC. 1987).
22. Olson, P. *Magma Transport and Storage* (ed. Ryan, M. P.) 33–51 (Wiley, New York, 1990).
23. Turcotte, D. L. & Schubert, G. *Geodynamics: Applications of Continuum Physics To Geological Problems* (Wiley, New York, 1982).
24. Olson, P., Schubert, G. & Anderson, C. *Nature* **327,** 409–413 (1987).
25. Box, G. E. P. & Jenkins, G. M. *Time Series Analysis, Forecasting and Control* (Holden-Day, San Francisco, 1970).

ACKNOWLEDGEMENTS. We thank the captain, crew and the scientific parties of the RAPA and Gloria expeditions, and D. K. Smith, R. Batiza and E. E. Davis for reviewing the manuscript. This work was supported by US NSF.

Albanerpetontid amphibians from the Cretaceous of Spain

Gerard McGowan & Susan E. Evans

Evolutionary Anatomy Unit, Department of Anatomy and Developmental Biology (Rockefeller), University College London, Gower Street, London WC1E 6BT, UK

ALBANERPETONTIDS **are a group of enigmatic salamander-like fossil amphibians known from deposits of middle Jurassic to Miocene age across Euramerica and Central Asia. Throughout a long history they remained remarkably conservative but can be diagnosed by a suite of unique derived character states, including an anterior peg-and-socket joint between the mandibles, non-pedicellate tricuspate teeth, a distinctive polygonal dermal sculpture pattern, and a two-part craniovertebral joint analogous to that of amniotes. Previous interpretations have placed albanerpetontids within salamanders[1,2] or as a separate amphibian group[3,4]. We report here on the recovery of the first complete albanerpetontid specimens (including traces of skin and possible male courtship glands) from the early Cretaceous of Spain. The new material supports the interpretation of albanerpetontids as predominantly terrestrial animals. Albanerpetontids resemble salamanders only in retaining an unspecialized tailed body form; cladistic analysis suggests they represent a distinct lissamphibian lineage.**

Albanerpetontids were formally described and named on the basis of disarticulated amphibian bones from the Miocene locality of Grive-St-Alban, France[5]. Although originally linked with the Cretaceous salamander *Prosiren*[1,6,7], and often classified within salamanders (Caudata)[1,2], some workers have contested this interpretation[3,4]. Between the earliest record (an atlas from the Middle Jurassic, Bajocian, of France[8]) and apparent extinction in the Miocene, albanerpetontids have been recorded from localities across North America, Europe and Central Asia[6,9,10], almost always in the form of dissociated elements. Until now, the only articulated specimen was a poorly known partial skeleton (the holotype of *Albanerpeton megacephalus*) from the early Cretaceous locality of Pietraroia in Italy[6].

The early Cretaceous (Barremian) Lithographic Limestone locality of Las Hoyas, near Cuenca, Spain, has yielded a rich freshwater/terrestrial assemblage including plants, aquatic invertebrates, insects, fish, frogs, salamanders, turtles, lizards, crocodiles, dinosaurs and birds[11–14]. The same deposits have now produced two complete albanerpetontids, one (LH 6020) with exquisite preservation of both hard and soft parts (Fig. 1*a–c*).

LH 6020 is the skeleton of a small, tailed amphibian of roughly 50 mm snout–vent length. The skeleton is fully ossified and ultraviolet light photography reveals the presence of body scales (Fig. 1*a*, *b*). The skin of the head, including the eyelids, contains a mosaic of small polygonal osteoderms, a feature that explains the distinctive skull ornament (Fig. 2*a*). The structure of the skull itself supports previous reconstructions[5], but a jugal is recorded for the first time and the slender spike-like form of the cultriform process of the parasphenoid is confirmed. In the axial skeleton, the atlas/axis complex (comprising a bicotylar atlas and a small free axis centrum) is followed by twenty holospondylous presacral vertebrae bearing single-headed ribs, a single sacral vertebra and at least 24 caudals. The scapula and coracoid remain separate and the scapula bears a long anteriorly directed process which braced the limb against the spine. The forelimb is strong, with an ossified radial ball on the humerus and a four-digit manus. In the pelvis, the pubis, ilium and ischium are all ossified. Unfortunately, the hands and feet are contracted (presumably as a result of post-mortem desiccation), making accurate reconstruction difficult. The carpal and tarsal series include three proximal, two or more central and a full set of distal elements. In the hand, the estimated phalangeal formula is 2:3:3:3; in the foot, it approximates 2:3:4/5:3:3.

Within the skin on the anterior surface of each thigh, just proximal to the knee, there is a discrete mass of about 100 small spherules (Fig. 1*c*). The most reasonable interpretation is of a glandular mass which possibly produced secretions designed to assist grip during courtship. If this is correct, the specimen would be male.

In general, the morphology (tough skin, heavy ossification, powerful limbs and girdles) supports the view[5] that albanerpetontids were predominantly terrestrial animals.

Comparison of the Las Hoyas albanerpetontid with those of Grive-St-Alban and Pietraroia suggest that the prevailing concept of the genus *Albanerpeton* extending from the Jurassic to the Miocene[1] is incorrect. There is a marked difference between the shape of the frontal in the type species *Albanerpeton inexpectatum*[1] and the related *A. galaktion*[3] (strongly triangular, narrow apex, broad, unemarginated orbital margins) and those of the Pietraroia and Las Hoyas specimens (waisted and more rectangular, bulbous apex, curved orbital margins) (Fig. 3*a–d*). No two species within a modern genus show this degree of difference and it seems a secure basis for generic distinction (other albanerpetontids will be discussed elsewhere). More subtle differences between the Pietraroia and Las Hoyas specimens in the shape of the internasal process and the prefrontal region (see below) suggest that they may be specifically distinct.

Family Albanerpetontidae[3]

Celtedens gen.nov.

Etymology. *Celtes* (Latin)—chisel; and *dens* (Latin)—tooth; an allusion to the shape of the teeth.

Type species. *Celtedens megacephalus* (=*Albanerpeton megacephalus*[6]).

Generic diagnosis. An albanerpetontid characterized by a waisted frontal with narrow, embayed orbital margins. The internasal process differs from that of *Albanerpeton sensu stricto* in being bulbous rather than spike-like.